Monthly Notices of the ROYAL ASTRONOMICAL SOCIETY

MNRAS **537,** 2579–2585 (2025) https://doi.org/10.1093/mnras/staf163
Advance Access publication 2025 January 31

Discs around young free-floating planetary-mass objects: ultradeep *Spitzer* imaging of IC348

Holly Hanbee Seo and Aleks Scholz ★

SUPA, School of Physics & Astronomy, University of St Andrews, North Haugh, St Andrews KY169SS, UK

Accepted 2025 January 22. Received 2025 January 10; in original form 2024 August 28

ABSTRACT

Protoplanetary discs have been found around free-floating objects with masses comparable to those of giant planets. The frequency and properties of these discs around planetary-mass objects are still debated. Here, we present ultradeep mid-infrared images for the young cluster IC348, obtained through stacking of time-series images from *Spitzer*. We measure fluxes at 3.6 and 4.5 μm for known free-floating planetary-mass objects (FFPMOs, spectral type M9 or later) in this cluster. By comparing the observed infrared spectral energy distributions with photospheric templates, we identify six planetary-mass objects with discs, plus three, which may or may not have a disc. This corresponds to a disc fraction of $46\pm^{13}_{12}$ per cent. The disc fraction among planetary-mass objects is comparable to more massive brown dwarfs. We show the disc fraction among FFPMOs as a function of age, demonstrating that these objects retain discs for several million years, similar to low-mass stars and brown dwarfs.

Key words: protoplanetary discs – brown dwarfs – stars: formation.

1 INTRODUCTION

It is now common knowledge that our Galaxy hosts a large number of brown dwarfs (perhaps 100 billion altogether; Mužić et al. 2017), as well as numerous isolated objects with masses around or below the Deuterium burning limit. First discovered in 2000 (Lucas & Roche 2000; Zapatero Osorio et al. 2000), these free-floating planetary-mass objects (FFPMOs) have now been found in nearby young clusters, associations, as well as in microlensing surveys (Scholz et al. 2012; Clanton & Gaudi 2017; Miret-Roig et al. 2022). The prevalence of FFPMOs is still under debate, as is their origin. Some of them could be the lowest mass objects to form like stars, others may be ejected planets. Future direct imaging and microlensing studies are expected to help us characterize the population of FFPMOs in the Galaxy (Scholz et al. 2022; Sumi et al. 2023).

The majority of stars, as well as most brown dwarfs, start their lives with a circum-(sub)-stellar accretion disc that lasts for one or more million years. In many cases, planets will form from the raw material in the discs, giving rise to the rich and diverse population of planetary systems established by exoplanet surveys (Cassan et al. 2012). The early signs of planet formation in the discs – in the form of grain growth and gap formation – have been found down to central object masses below 0.1 $M_\odot$ (Scholz et al. 2007; Pinilla et al. 2018). Moreover, the discs themselves have been identified around objects with masses as low as 0.01 $M_\odot$, or $\sim 10 M_{\rm Jup}$ (Luhman et al. 2005b; Joergens et al. 2013; Damian et al. 2023; Scholz et al. 2023). The standard way to identify discs is by looking for infrared excess emission at wavelengths >2 μm, an approach that has benefitted from the wide availability of sensitive coverage of star-forming regions by the *Spitzer Space Telescope* (Werner et al. 2004).

Here, we investigate the prevalence and lifetimes of discs around young FFPMOs, using ultradeep images created by stacking archival *Spitzer* data. This paper is a direct follow-up to a previously published study with similar approach and goals, which was focused on the young cluster NGC1333 (Scholz et al. 2023). Our target for this paper is IC348, the second major cluster in the Perseus star-forming complex (Luhman, Esplin & Loutrel 2016; Pavlidou, Scholz & Teixeira 2021). With nearly 500 cluster members and a quoted age of 3–5 Myr, IC348 is larger and slightly older than its sibling NGC1333. As in Scholz et al. (2023), we use *Spitzer*/IRAC time-series imaging to produce ultradeep images of the cluster, and measure infrared fluxes for sub-stellar members (Section 2). We identify planetary-mass objects (PMOs) with discs, derive the disc fraction, and compare with the literature (Section 3). We present our conclusions in Section 4.

2 DATA PROCESSING

2.1 Stacking of *Spitzer* images

The cluster IC348 was observed by *Spitzer* several times. Here, we make use of a time series obtained during the 'warm mission', in cycle 9, as part of the programme with the ID 60160 (PI: Muzerolle). Altogether, 38 images were taken in the IRAC1 and IRAC2 channels, at wavelengths of 3.6 and 4.5 μm (Fazio et al. 2004), and at a constant position. The observations are spread out over 40 d in late 2009. The primary scientific purpose of this programme was to study variability, with the results reported in Flaherty et al. (2011, 2012). Here, we stack all data for a given channel to produce an ultradeep image of the cluster. The single-frame exposure time is 12 s, identical to

★ E-mail: as110@st-andrews.ac.uk

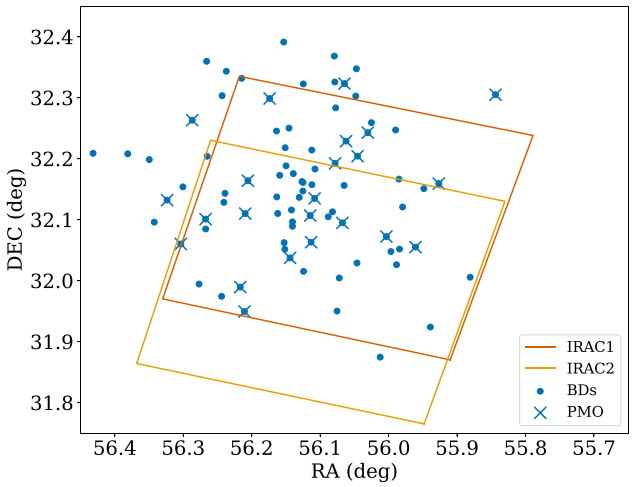

Figure 1. Spatial distribution of brown dwarfs in IC348, defined as spectral type M6 or later. 'In boxes', we show the approximate coverage of the fields in IRAC1 and IRAC2 for the stacked image used in this paper. We mark the PMOs with spectral type M9 or later.

single-epoch mosaics obtained for IC348 for the 'Cores to Disks' programme (Evans et al. 2009). That means, the stack will have a combined on-source time of 456 s (or 7.6 min).

We downloaded all 38 images per channel from the Spitzer Heritage Archive. These two sets were stacked using the PYTHON package REPROJECT, a part of ASTROPY. The full stacked image covers approximately 0.4×0.4 degrees, including the majority of the known cluster members. The central J2000.0 coordinates in IRAC1 are (56.08, 32.10) and (56.12, 32.00) in IRAC2. The pixel scale of the stacks, as well as the individual images, is 0.6 arcsec. By stacking 38 images, the signal-to-noise ratio should be improved by about $\sqrt{38} = 6.16$, which means the resulting image should be about 2 mag deeper than an individual epoch.

2.2 Brown dwarf sample

To define our sample, we use the census for this cluster from Luhman et al. (2016), which encompasses in total 478 stars and brown dwarfs classified as members of IC348. According to the authors, the survey is 'nearly complete' down to K-band magnitudes of 16.8 and J-band extinction $A_J = 1.5$. For our purposes, we selected the subsample of objects with spectral types of M6 or later. According to evolutionary tracks, this spectral type corresponds to a mass around 0.1 $M_\odot$ for ages of 1–5 Myr; hence, our subset should include all spectroscopically confirmed brown dwarfs in this census. In this paper, however, we are primarily interested in the sources with spectral types M9 or later, which is likely to correspond to masses around or below the Deuterium burning limit at young ages.

In total, we select 83 objects with adopted spectral type of M6.0 or later. Of these, 23 have spectral type of M9 or later. From this subsample, 67 are covered by our deep *Spitzer* images, 19 of which have spectral type of M9 or later. Due to the offset between the two IRAC channels, some objects are only covered in one band. In addition, some objects are located too close to the edges for reliable measurements, those will not be used in the following. Overall, this results in 17 objects with M9 or later spectral type and valid measurements. Four of those are only covered in IRAC1. In Fig. 1, we show the spatial distribution of the sample, compared to the fields covered by our deep IRAC1 and IRAC2 images. We note that a recent *JWST* survey uncovered a couple more objects, which may be planetary-mass members of IC348 (Luhman et al. 2024), but are too faint to be included here.

2.3 Photometry

We measured fluxes for the brown dwarfs in the images using Bradley et al. 2021PHOTUTILS. For the circular apertures, we used a radius of 5 pixels (or 3 arcsec). The background was estimated as the median in a circular annulus between radii of 7 and 9 pixels. After converting to magnitudes, those were calibrated by cross-matching with the catalogue by Gutermuth et al. (2009), which includes the IC348 region.

To calculate extinction-free colours, we dereddened the IRAC1 and IRAC2 photometry, using the extinction measurements provided by Luhman et al. (2016). Their paper lists A_J, calculated from A_V with the Cardelli, Clayton & Mathis (1989) extinction law ($A_J = 0.28 A_V$). We re-derived A_J using the more recent extinction law from Wang & Chen (2019) ($A_J = 0.243 A_V$). We used the same extinction law to deredden the photometry in the IRAC bands. We dereddened the published K-band photometry by Luhman et al. (2016) using the same process.

The median photometric error for our sample is 0.07 mag. For faint objects, the photometric error can be significantly larger; for the PMOs in our sample, the error in the IRAC photometry is up to 0.2 mag. As additional error from the calibration we adopt 0.01 mag. Also, the extinction correction adds a small uncertainty, which combines the error in A_V ($\sim$0.5 mag) and the negligible error in the band coefficient (0.003–0.004 mag). The magnitudes and dereddened colours for all PMOs in our sample are listed in Table 1.

3 DISCS IN PLANETARY-MASS OBJECTS

3.1 Infrared colour excess

Circum-sub-stellar discs are routinely identified by looking for infrared colour excess caused by warm dust in the inner parts of the discs. Here, we use the K − IRAC colour (combining our IRAC photometry with the K-band magnitudes from Luhman et al. 2016) as an initial indicator for the presence of a disc. For brown dwarfs and PMOs with temperature below 3000 K, the K-band magnitudes at a wavelength of 2.2 μm are dominated by the photosphere. On the other hand, the IRAC magnitudes at wavelengths of 3.6 and 4.5 μm are affected by excess emission from the disc, if present (e.g. Natta & Testi 2001). Overall, the K − IRAC1 and K − IRAC2 colours should show excess above the photosphere, if a disc is present.

In Fig. 2, we show the dereddened K − IRAC2 and K − IRAC1 colours as a function of spectral type for our sample. In K − IRAC2, we see two populations of objects forming two sequences. The population with elevated colour should correspond to objects with discs. In K − IRAC1, the division is not clear, and it is difficult to disentangle objects with and without excess. This is expected; the signature of the discs should become more distinctive at longer wavelengths. In the following, we will therefore use exclusively the K − IRAC2 colour.

To robustly identify a colour excess requires an estimate of the photospheric colour. We use the polynomial relations from Sanghi et al. (2023) published in their table A1, for this purpose. They provide relations for absolute magnitude versus spectral type for brown dwarfs in young moving groups. Instead of the IRAC bands, they present relations for the WISE bands at similar wavelengths ($W1$

Table 1. New *Spitzer* photometry for PMOs in IC348. Spectral type, A_J, and K are from Luhman et al. (2016), but the extinction has been adjusted with the more recent extinction law by Wang & Chen (2019). The colours are dereddened to $A_J = 0$, and are identical to the values plotted in Fig. 2.

UGCS	LRL	SpT	A_J	K	$I1$	$I2$	K − IRAC1	K − IRAC2
J034350.58+320317.5	1843	M9	2.17	15.19	13.89 ± 0.06	13.34 ± 0.06	0.94 ± 0.09	1.38 ± 0.09
J034416.18+320541.0	4044	M9	0.47	17.09	15.20 ± 0.11	14.75 ± 0.11	0.81 ± 0.13	1.24 ± 0.13
J034427.18+320346.6	705	M9	0.35	15.73	14.99 ± 0.10	14.83 ± 0.12	0.68 ± 0.12	0.83 ± 0.13
J034504.17+320602.9		M9	0.00	16.87	16.04 ± 0.17	15.97 ± 0.20	0.83 ± 0.18	0.90 ± 0.21
J034449.33+320949.4		M9	0.10	16.56	15.82 ± 0.15	15.74 ± 0.18	0.72 ± 0.16	0.80 ± 0.19
J034449.33+320949.4	40023	M9.5	0.39	16.88	15.76 ± 0.15	15.56 ± 0.17	1.05 ± 0.16	1.24 ± 0.18
J034450.24+320635.5	5231	M9.5	0.00	17.39	16.65 ± 0.22	16.06 ± 0.21	0.74 ± 0.23	1.33 ± 0.22
J034451.99+315921.6	1379	M9.7	0.29	15.86	14.95 ± 0.10	14.57 ± 0.11	0.86 ± 0.12	1.23 ± 0.12
J034400.75+320420.0	40142	L0	0.00	17.69	16.76 ± 0.23	16.51 ± 0.26	0.93 ± 0.24	1.18 ± 0.27
J034450.52+315657.3		L0	0.00	16.39	15.68 ± 0.14	15.55 ± 0.17	0.71 ± 0.16	0.84 ± 0.18
J034427.47+320624.2	30057	L1	0.49	18.06	16.72 ± 0.23	16.17 ± 0.22	1.23 ± 0.24	1.79 ± 0.23
J034425.92+320805.4	6005	L1	0.49	17.54	16.66 ± 0.22	16.17 ± 0.22	0.80 ± 0.23	1.26 ± 0.23
J034434.54+320213.7	5209	L1	0.49	17.48	16.63 ± 0.22	16.31 ± 0.24	0.77 ± 0.23	1.06 ± 0.25

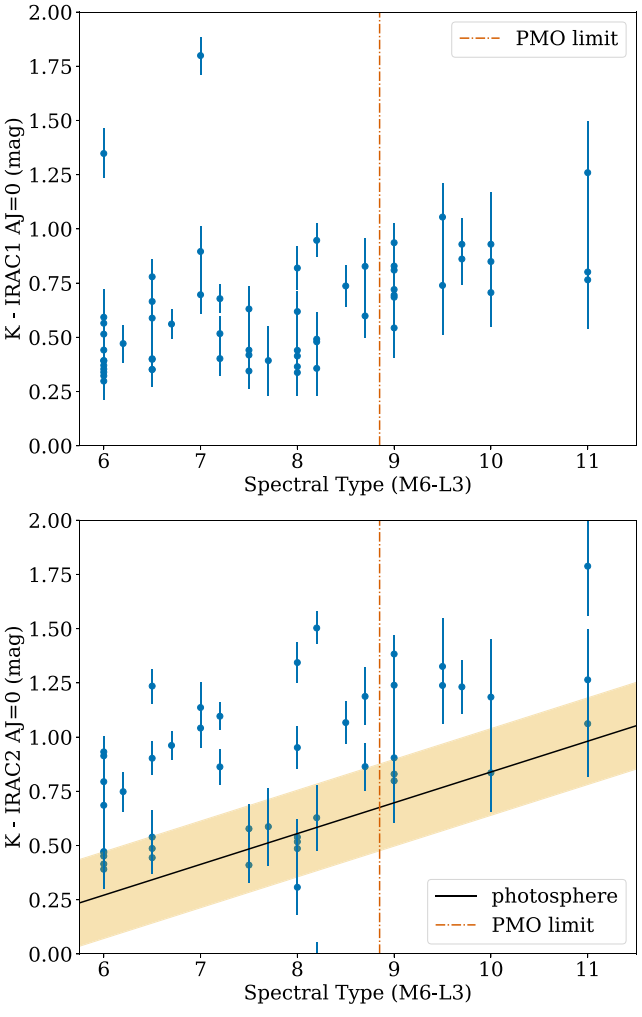

Figure 2. K − IRAC infrared colours versus spectral type for all objects with valid measurements. In this paper, we primarily focus on the objects with spectral types M9 or later, on the right side of the dash–dotted line. For K − IRAC2, the separation between objects with/without discs is apparent; for this panel, we also overplot the photospheric colours. For more details, see text.

and $W2$). We compared the IRAC with WISE photometry for young, cool stars and brown dwarfs from a sample in the Upper Scorpius star-forming region (Esplin et al. 2018). This region is slightly older than IC348 and the overwhelming majority of the objects do not show excess emission. The K − IRAC2 colour in that sample follows closely the $K - W2$ colour, confirming that using the Sanghi et al. (2023) relations for WISE is valid for estimating the photospheric colours. We note that this relation is also comparable to the one adopted in Scholz et al. (2023), which was based on an independent study but does not extend beyond spectral types L1.

As a side note, using the same approach we find a significant offset of ∼0.2 mag between the $K - W1$ and the K − IRAC1 colours. The $W1$ and IRAC1 bands are similar (Jarrett et al. 2011), but not identical. Late M to early L dwarfs feature broad absorption due to water in this band (Cushing, Rayner & Vacca 2005), which means that small changes in the band limits can affect the colours. Conversely, in the IRAC2 band the spectrum for late M/early L objects is essentially a smooth slope (Manjavacas et al. 2024), which simplifies band conversions.

The photospheric values are shown as black line in the lower panel of Fig. 2, with an indicative uncertainty as yellow band. The plot clearly demonstrates that some of the sources show colour excess above the photosphere; i.e. their colours are located above the range expected for a pure photosphere. To reiterate, all objects in these plots were checked individually in the images, to ensure that close neighbours, nearby edges, and varying background do not affect the flux measurements. Judged by the K − IRAC2 colour, the fraction of sources with infrared excess and spectral type of M9 or later is a maximum of 9 of 13, with considerable uncertainty. In the following, we scrutinize these nine potential PMOs with discs more in detail. For the brown dwarfs with M6–M8 spectral type, the disc fraction would be around 50 per cent according to this figure, with a few objects that are difficult to classify. As we will discuss later, this disc fraction is in line with previous estimates for the mid-to-late M dwarfs in this cluster.

3.2 Spectral energy distributions

To verify the presence of discs in the sources with spectral types M9 or later, we combine our photometry at 3.6 and 4.5 μm with literature data. In particular, we use the deep J, H, and K photometry from UKIDSS-DR9 (Lawrence et al. 2007, 2013), which is available

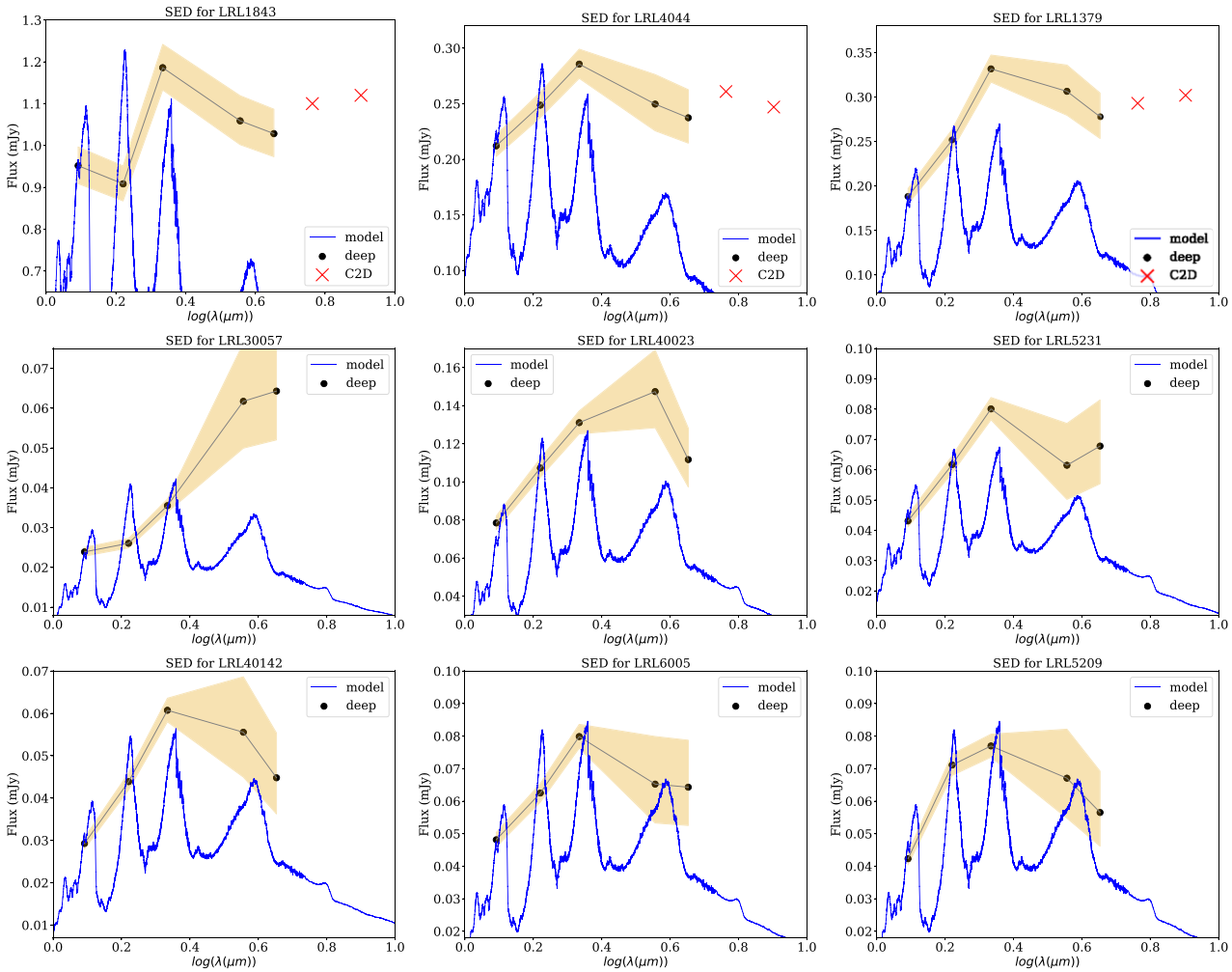

Figure 3. Spectral energy distributions for planetary-mass brown dwarfs with potential excess emission due to discs. The black, connected data points are based on dereddened photometry, with the data points at 3.6 and 4.5 μm from this study. The yellow shaded region indicates the error; here, we adopt a conservative error of 5 per cent for the JHK photometry. The spectrum plotted in blue comes from models used as templates. When available, we also show the C2D data points at 5.8 and 8.0 μm in red. See text and Table 2 for details.

for all objects in our sample. For the very faintest source, we use the *J*-band magnitude from Preibisch, Stanke & Zinnecker (2003). Whenever we found multiple valid measurements for the same band, we verified that they are in agreement with each other. We deredden the UKIDSS and our IRAC magnitudes, using the values of A_J used earlier and the Wang & Chen (2019) extinction law, and convert to flux densities F_ν in mJy. In addition, if available, we add the *Spitzer* fluxes at 5.8 and 8.0 μm from the C2D Full Clouds Catalogue (Evans et al. 2009). In general, if a flux has been measured by C2D at 5–8 μm, it is a clear confirmation of a disc. The photospheric fluxes for objects in IC348 at those spectral types are too low beyond 5 μm to be detected robustly by *Spitzer*. To unambiguously identify a disc, we demand that the excess is seen in at least two bands.

As a template for the photospheric emission, we use here model spectra from the BT-Settl-AGSS series (Allard et al. 2007; Asplund et al. 2009), for $\log g = 3.5$ and effective temperatures ranging from 1500 to 2500. According to Sanghi et al. (2023) (see their fig. 16), this temperature range should cover the spectral type range considered here. Models are smoothed and scaled to the dereddened near-infrared fluxes of our targets. We varied the temperature until we achieve a good match between the model and the fluxes in *J* and *H* bands, which would represent the photosphere. The outcomes described below do not depend on the specific choice of model spectra within those parameters.

In Fig. 3, we show the spectral energy distributions for all PMOs with potential disc detection, with errors as shaded region. In Table 2, we report the data used for these figures, plus the $T_{\rm eff}$ value of the model chosen as comparison. Based on this analysis, five of these nine objects are unambiguously classified as having infrared excess, evidence for a circum-sub-stellar disc. For all five, there are multiple measurements significantly above the photospheric flux. For three of these, at least one data point at 5–8.0 μm exists and confirms the excess. For one more, there is marginal excess emission and an increasing SED; we add this to the sample with discs. For the remaining three, the figures do not show evidence for excess emission. The other four objects with spectral type of M9 or later in our deep images also have colours consistent with a pure photosphere. To reiterate, this does not preclude the presence of a disc; they could still harbour a disc with an inner hole and excess at wavelengths longer than 8 μm.

Table 2. PMOs in IC348 with potential disc. JHK photometry is from UKIDSS [except *J* band from Preibisch et al. (2003) for LRL30057]. Spectral type and A_J are from Luhman et al. (2016). IRAC photometry is from this paper. T_{eff} is the effective temperature of the model spectrum used for comparison in Fig. 3. 'C2D' indicates whether there are measurements from C2D at 5.8 and/or 8.0 μm. The column 'Disc' indicates whether or not there is evidence for a disc.

UGCS	LRL	SpT	A_J	J	H	K	$I1$	$I2$	T_{eff}	C2D	Disc
J034350.58+320317.5	1843	M9	2.17	17.73	16.30	15.07	13.89	13.34	2200	yes	yes
J034416.18+320541.0	4044	M9	0.47	17.66	16.79	16.07	15.20	14.75	2100	yes	yes
J034451.99+315921.6	1379	M9.7	0.29	17.61	16.68	15.85	14.95	14.56	2000	yes	yes
J034427.47+320624.2	30057	L1	0.49	20.05	19.25	18.34	16.72	16.17	1900	no	yes
J034449.33+320949.4	40023	M9.5	0.39	18.66	17.66	16.89	15.76	15.56	1900	no	yes
J034450.24+320635.5	5231	M9.5	0.0	18.92	18.05	17.30	16.65	16.06	2000	no	yes
J034400.75+320420.0	40142	L0	0.0	19.34	18.42	17.60	16.76	16.51	1900	no	no?
J034425.92+320805.4	6005	L1	0.49	19.29	18.30	17.46	16.66	16.17	1900	no	no?
J034434.54+320213.7	5209	L1	0.49	19.43	18.16	17.50	16.63	16.31	1900	no	no?

3.3 Comments on individual objects

In the following, we provide some commentary on individual sources.

LRL1843 has clear excess flux in the IRAC bands, compared to all templates with 2000–2500 K. The excess emission also exceeds the (small) error in the infrared fluxes. The presence of the disc is also confirmed by robust detections at 5.8 and 8.0 μm, with fluxes around 1 mJy. Infrared excess has also been identified by Luhman et al. (2016) for this object. It is a clear detection of a disc. Note that the near-infrared fluxes do not match very well with the model spectra; this may be due to an overestimate in the extinction (which is the highest in this sample).

LRL4044 shows clear excess in our IRAC measurements above the templates with plausible temperature. It also has a detection at 5.8 μm in C2D (but only an upper limit at 8.0 μm). The SED is flat out to 6 μm, whereas the photospheric template fluxes drop off quickly in the mid-infrared. This is a clear disc detection.

LRL1379 shows significant excess emission from 3 to 8 μm, including robust detections in the C2D survey. There might already be excess emission in the *K* band. The infrared excess was already identified in Luhman et al. (2016). The object is clearly harbouring a circum-sub-stellar disc.

LRL30057 has a rising SED from 1 to 4.5 μm, and substantial excess emission over photospheric templates at temperatures of 1900 K or similar. The SED shows all characteristics of a Class II source with a flared disc. It is not robustly detected at longer wavelengths, but this is not surprising given how faint the source is. This object is regarded a safe disc detection.

LRL40023 has an SED that peaks at 3.6 μm, in terms of F_ν. It shows significant excess emission in IRAC1 and IRAC2, but has no robust C2D detection at longer wavelengths. In agreement with Luhman et al. (2016), we still consider this object to be a safe disc detection, despite the decline in the flux level at 4.5 μm.

LRL5231 has marginal excess emission in IRAC1, and substantial excess in IRAC2, compared to the 2000 K template. There may be slight excess emission in the *K* band as well. The flux at 4.5 μm is comparable or higher than at 3.6 μm, while the photospheric flux drops sharply at 4 μm. Based on those facts, we consider it likely that the source harbours a disc. It is the only one where our classification disagrees with Luhman et al. (2016).

LRL40142 has slightly elevated flux levels at 3.6 and 4.5 μm, compared to the 1900 K template. Choosing a template with a slightly higher or lower temperature does not change the basic outcome. The SED peaks in the *K* band, and fluxes drop towards longer wavelengths. There are no useful fluxes from C2D at wavelengths >5 μm. Given that the SED declines it is reasonable to assume that the object does not have a disc.

LRL6005 and LRL5209 have infrared fluxes that are largely consistent with the photosphere, within the considerable margin of error. Their SEDs are declining beyond the *K* band. There are no C2D data points for longer wavelengths. In both cases, we use the 1900 K model as template, but the specific choice does not change the outcome. It is unlikely that any of these two has excess emission due to a disc based on the available data.

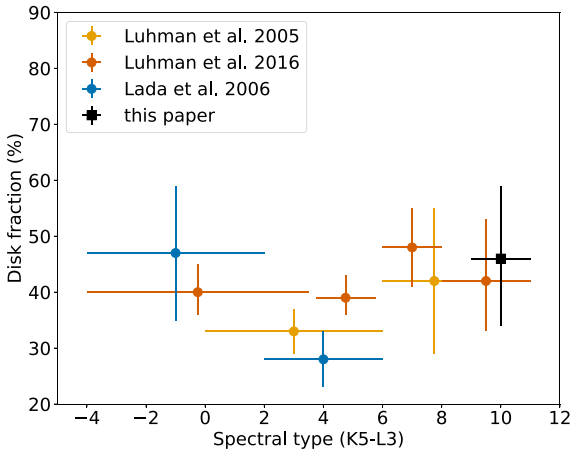

Figure 4. Disc fraction in IC348 as a function of spectral type, including our new data points for PMOs. The data shown are from Lada et al. (2006), Luhman et al. (2005a), and Luhman et al. (2016). For our estimate in black, we show the lower and upper limits.

3.4 Disc fractions

In this paper, we have used the spectral type limit of M9 as a proxy for mass – all 23 brown dwarfs with M9 or later in the Luhman et al. (2016) census are considered to be possible PMOs in IC348. For 13 of these, we present new photometry from deep IRAC1 and IRAC2 images. For this subsample, we test for the presence of a disc using the same consistent method. We find that six of those have a disc, corresponding to a disc fraction of 6/13 or 46 per cent. The uncertainty for this value was estimated by calculating how likely it is to observe 6 successes out of 13 trials, assuming a binomial distribution and a flat prior. This gives us a 1σ confidence interval of 34–59 per cent, which means that the disc fraction is 46^{+13}_{-12} per cent.

In Fig. 4, we plot disc fractions for IC348 as a function of spectral types, including results from the literature combined with our new

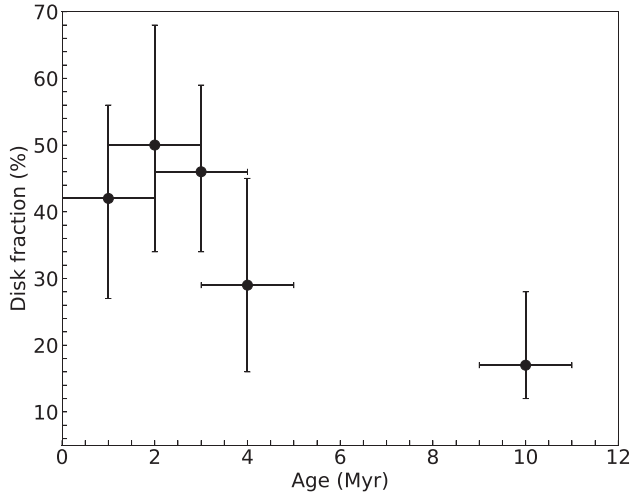

Figure 5. Disc fraction among FFPMOs as a function of age. Included are data points for NGC1333 (1 Myr; Scholz et al. 2023), Chamaeleon-I (2 Myr; Luhman et al. 2008), IC348 (3 Myr; this paper), σ Orionis (4 Myr; Scholz & Jayawardhana 2008), and Upper Scorpius (10 Myr; Luhman & Mamajek 2012). Note that these are typical ages for these regions, and the uncertainty is approximately $\pm$1 Myr.

data point for planetary-mass sources. From Lada et al. (2006), we plot disc fractions of 47 $\pm$ 12 per cent for spectral types K6–M2 and 28 $\pm$ 5 per cent for M2–M6. Here, we only consider the values for full discs, as anaemic discs, as classified by the authors, would be difficult to identify for faint late M/early L type objects. Also included are the values from Luhman et al. (2005a) who measured 33 $\pm$ 4 per cent for M2–M6 and 42 $\pm$ 13 per cent for M6–M9. The Luhman et al. (2016) census gives disc fractions of 39 per cent for mid-M, 48 per cent for M6–M8, and 42 per cent for later-type objects, with associated error bars; these data points are also included in our figure.

As seen in this figure, our data point is in agreement with all previous measurements of the disc fraction in the brown dwarf domain, within the (substantial) error bars. It is very similar to the value for >M8 objects published in Luhman et al. (2016). As already mentioned, our indicative estimate of ~50 per cent for M6–M9 objects is also in line with previous measurements.

The plot does show an overall trend of disc fraction with spectral type – the disc fraction drops slightly from around 50 per cent to 30 per cent from mid-K to early M spectral types (already noticed in the literature), but then rises slightly towards late M spectral types. A trend of increasing disc fraction with later spectral type has been noted for low-mass stars and brown dwarfs in the older Upper Scorpius star-forming region (Luhman & Mamajek 2012), but based on a small sample size. It may be an indication that discs among very low mass brown dwarfs live longer than in more massive objects.

With the new data point in IC348, we also have an opportunity to probe the evolution of discs around PMOs over time. In Fig. 5, we show disc fractions for five star-forming regions, NGC1333 (Scholz et al. 2023), Chamaeleon-I (Luhman et al. 2008), IC348 (this paper), σ Orionis (Scholz & Jayawardhana 2008), and Upper Scorpius (Luhman & Mamajek 2012). The numbers are plotted at approximate ages, typical for ages cited in the literature, but the uncertainty (or spread) in age is at the minimum 1 Myr. In all regions, the disc fractions have been determined for a spectral type range comparable to the one probed here (i.e. either M9 or later or M8 or later). Since disc fraction does not depend strongly on spectral type (see above), using those data points together is not introducing a bias. In all regions, the disc fractions are estimated at 3–5 μm; i.e. the data points should be comparable. As shown by this plot, disc fractions for PMOs stay in the 40–50 per cent range for at least 3–4 Myr before they significantly drop off. Thus, the disc lifetime in PMOs is not strongly different from that in brown dwarfs or low-mass stars (Haisch, Lada & Lada 2001; Manara et al. 2023).

4 SUMMARY

In this paper, we search for discs around PMOs in the young cluster IC348. The study is based on deep *Spitzer* images, created by stacking 38 archival images taken for a time-series study. The images cover 13 previously identified young brown dwarfs with spectral types of M9–L3, corresponding to masses below or around the Deuterium burning limit. This is the core sample for this paper.

We measure infrared fluxes at 3.6 and 4.5 μm for our sample. Based on the $K - [4.5]$ μm colour, 9 of those 13 objects show signs of excess emission. We further examined these by comparing the full spectral energy distribution with model spectra. Six of them we classify as objects with discs, with multiple data points showing excess emission above the photosphere. The remaining three have SEDs largely consistent with a photosphere. The disc detections are excellent targets for future detailed studies of discs around PMOs.

The disc fraction in our sample is 6/13 or 46 per cent. This is entirely consistent with previous estimates in the literature for a similar spectral type range. PMOs at ages of a few Myr have disc fractions comparable to higher mass brown dwarfs and low-mass stars. About a third to half of them retain their discs for several million years. The long-lived discs identified here may signal that there might be planets around objects, which themselves have masses comparable to giant planets.

ACKNOWLEDGEMENTS

We thank the anonymous referee for a constructive review that helped to improve this paper. AS acknowledges support from the UKRI Science and Technology Facilities Council through grant ST/Y001419/1/. This research has made use of the VizieR catalogue access tool, CDS, Strasbourg, France (DOI: 10.26093/cds/vizier). The original description of the VizieR service was published in A&AS, 143, 23 (2000).

DATA AVAILABILITY

The imaging data underlying this article were accessed from the Spitzer Heritage Archive, at https://irsa.ipac.caltech.edu/applications/Spitzer/SHA/. In addition, data from peer-reviewed papers are used, all cited in this paper. The data for the colour–magnitude plots in Fig. 2 are included in Table 1. The data for the spectral energy distributions in Fig. 3 are contained in Table 2.

REFERENCES

Allard F., Allard N. F., Homeier D., Kielkopf J., McCaughrean M. J., Spiegelman F., 2007, A&A, 474, L21
Almendros-Abad V., Mužić K., Moitinho A., Krone-Martins A., Kubiak K., 2022, A&A, 657, A129
Alves de Oliveira C., Moraux E., Bouvier J., Bouy H., 2012, A&A, 539, A151
Asplund M., Grevesse N., Sauval A. J., Scott P., 2009, ARA&A, 47, 481
Baraffe I., Homeier D., Allard F., Chabrier G., 2015, A&A, 577, A42

Bayo A. et al., 2017, ApJ, 841, L11
Bradley L. et al., 2021, astropy/photutils: 1.3.0. Zenodo
Cardelli J. A., Clayton G. C., Mathis J. S., 1989, ApJ, 345, 245
Cassan A. et al., 2012, Nature, 481, 167
Clanton C., Gaudi B. S., 2017, ApJ, 834, 46
Cushing M. C., Rayner J. T., Vacca W. D., 2005, ApJ, 623, 1115
Damian B., Jose J., Biller B., Paul K. T., 2023, JA&A, 44, 77
Esplin T. L., Luhman K. L., Miller E. B., Mamajek E. E., 2018, AJ, 156, 75
Evans N. J.,, II et al., 2009, ApJS, 181, 321
Fazio G. G. et al., 2004, ApJS, 154, 10
Flaherty K. M., Muzerolle J., Rieke G., Gutermuth R., Balog Z., Herbst W., Megeath S. T., Kun M., 2011, ApJ, 732, 83
Flaherty K. M., Muzerolle J., Rieke G., Gutermuth R., Balog Z., Herbst W., Megeath S. T., Kun M., 2012, ApJ, 748, 71
Gutermuth R. A., Megeath S. T., Myers P. C., Allen L. E., Pipher J. L., Fazio G. G., 2009, ApJS, 184, 18
Haisch K. E., Lada E. A., Lada C. J., 2001, ApJ, 553, L153
Jarrett T. H. et al., 2011, ApJ, 735, 112
Joergens V., Bonnefoy M., Liu Y., Bayo A., Wolf S., Chauvin G., Rojo P., 2013, A&A, 558, L7
Lada C. J. et al., 2006, AJ, 131, 1574
Lawrence A. et al., 2007, MNRAS, 379, 1599
Lawrence A. et al., 2013, VizieR Online Data Catalog, 2319, II/319
Lucas P. W., Roche P. F., 2000, MNRAS, 314, 858
Luhman K. L., Mamajek E. E., 2012, ApJ, 758, 31
Luhman K. L. et al., 2005a, ApJ, 631, L69
Luhman K. L., Adame L., D'Alessio P., Calvet N., Hartmann L., Megeath S. T., Fazio G. G., 2005b, ApJ, 635, L93
Luhman K. L. et al., 2008, ApJ, 675, 1375
Luhman K. L., Esplin T. L., Loutrel N. P., 2016, ApJ, 827, 52
Luhman K. L., Alves de Oliveira C., Baraffe I., Chabrier G., Geballe T. R., Parker R. J., Pendleton Y. J., Tremblin P., 2024, AJ, 167, 19
Manara C. F., Ansdell M., Rosotti G. P., Hughes A. M., Armitage P. J., Lodato G., Williams J. P., 2023, in Inutsuka S., Aikawa Y., Muto T., Tomida K., Tamura M., eds, ASP Conf. Ser. Vol. 534, Protostars and Planets VII. Astron. Soc. Pac., San Francisco, p. 539
Manjavacas E. et al., 2024, AJ, 167, 168
Miret-Roig N. et al., 2022, Nat. Astron., 6, 89
Mužić K., Schödel R., Scholz A., Geers V. C., Jayawardhana R., Ascenso J., Cieza L. A., 2017, MNRAS, 471, 3699
Natta A., Testi L., 2001, A&A, 376, L22
Pavlidou T., Scholz A., Teixeira P. S., 2021, MNRAS, 503, 3232
Pinilla P., Natta A., Manara C. F., Ricci L., Scholz A., Testi L., 2018, A&A, 615, A95
Preibisch T., Stanke T., Zinnecker H., 2003, A&A, 409, 147
Sanghi A. et al., 2023, ApJ, 959, 63
Scholz A., Jayawardhana R., 2008, ApJ, 672, L49
Scholz A., Jayawardhana R., Wood K., Meeus G., Stelzer B., Walker C., O'Sullivan M., 2007, ApJ, 660, 1517
Scholz A., Jayawardhana R., Muzic K., Geers V., Tamura M., Tanaka I., 2012, ApJ, 756, 24
Scholz A., Muzic K., Jayawardhana R., Quinlan L., Wurster J., 2022, PASP, 134, 104401
Scholz A., Muzic K., Jayawardhana R., Almendros-Abad V., Wilson I., 2023, AJ, 165, 196
Sumi T. et al., 2023, AJ, 166, 108
Wang S., Chen X., 2019, ApJ, 877, 116
Werner M. W. et al., 2004, ApJS, 154, 1
Zapatero Osorio M. R., Béjar V. J. S., Martín E. L., Rebolo R., Barrado y Navascués D., Bailer-Jones C. A. L., Mundt R., 2000, Science, 290, 103

This paper has been typeset from a TEX/LATEX file prepared by the author.